ACS APPLIED MATERIALS & INTERFACES

Research Article

www.acsami.org

An Easily Accessible Donor–π-Acceptor-Conjugated Small Molecule from a 4,8-Dialkoxybenzo[1,2-*b*:4,5-*b*′]dithiophene Unit for Efficient Solution-Processed Organic Solar Cells

Pranabesh Dutta,[†] Jeongseok Kim,[†] Seung Hun Eom,[†] Woo-Hyung Lee,[‡] In Nam Kang,[‡] and Soo-Hyoung Lee*,[†]

[†]School of Semiconductor and Chemical Engineering, Chonbuk National University, Duckjin-dong 664-14, Jeonju 561-756, Republic of Korea

[‡]Department of Chemistry, The Catholic University, 43-1 Yeokaok-2-dong, Wonmi-gu, Buchen-si, Gyeonggi-do 420-743, Republic of Korea

ABSTRACT: A new donor–acceptor-conjugated organic small molecule, **BDT(TBT)$_2$**, comprised of benzo[1,2-*b*:4,5-*b*′]dithiophene and 2,1,3-benzothiadiazole units was designed and synthesized. The small molecule **BDT(TBT)$_2$** in its thin film showed an absorption band in the range of 300–700 nm with an absorption edge at 650 nm and an optical band gap of 1.90 eV. As estimated from the cyclic voltammetry measurements, the HOMO and LUMO energy levels of **BDT(TBT)$_2$** were −5.44 and −3.37 eV, respectively. The spin-coated thin film of **BDT(TBT)$_2$** exhibited p-channel output characteristics with a hole mobility of 2.7×10^{-6}. **BDT(TBT)$_2$**, when explored as an electron-donor material in solution-processed bulk-heterojunction organic solar cells in conjunction with a $PC_{71}BM$ acceptor with an active layer thickness of 50–55 nm, generated a power conversion efficiency (PCE) of 1.18%. A more impressive PCE of ∼2.9% with a short-circuit current density (J_{sc}) of 7.94 mA cm^{-2} and an open-circuit voltage (V_{oc}) of 0.89 V was achieved when the active layer of the cell was annealed at higher temperature (∼180 °C).

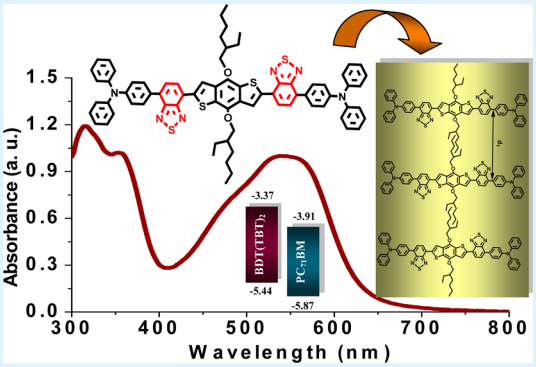

KEYWORDS: *organic solar cell, benzo[1,2-b:4,5-b′]dithiophene, donor–acceptor-conjugated small molecule, power conversion efficiency*

INTRODUCTION

Organic photovoltaic (OPV) technology is one of the most rapidly advancing areas of research in both academia and industry because of its potential for satisfying the growing demands of the world's increased energy needs. Until now, polymer solar cells (PSCs) consisting of blends of low-band-gap (LBG) donor–acceptor (D–A)-conjugated polymers and fullerene derivatives such as 6,6-phenyl-C61-butyric acid methyl ester ($PC_{61}BM$) or 6,6-phenyl-C71-butyric acid methyl ester ($PC_{71}BM$) as acceptors have shown great promise for the commercial production of inexpensive, lightweight, flexible photovoltaic cells with power conversion efficiencies (PCEs) exceeding 8%.[1−3] Toward the development of cost-effective OPV cells, in addition to conjugated polymers, the small molecules, which possess a number of advantages over their macromolecular counterparts including well-defined molecular weight and structure, easier purification and scale-up, greater purity, and reproducibility in batch-to-batch production, are also currently the focus of considerable interest. Continuous effort in recent years in the development of new D–A-conjugated small molecules has resulted in great accomplishments with solution-processed D–A-conjugated organic small molecules.[4−9] More than ever before, an impressive PCE of ∼7% has been achieved that truly demonstrates the potential of small molecules in OPV devices.[10] The development of new small molecules that incorporate well-matched D–A units is additionally expected to enhance the photovoltaic performance of the solution-processed small-molecular organic solar cell devices.

In D–A-conjugated polymers intended for photovoltaic applications, the benzo[1,2-*b*:4,5-*b*′]dithiophene (BDT) unit has thus far proven to be the most successful donor unit. Given the advantages of linear, symmetrical, and planar π-conjugated fused structures that promote a higher-ordered π stacking and improved hole mobility, a number of 4,8-dialkyl/dialkoxy-substituted BDT-based polymers have demonstrated excellent photovoltaic properties with PCEs greater than 7%.[11−14] More recently, an outstanding PCE of 8.37% has further been accomplished using the BDT-based polymers PTB7.[15] However, while extensive efforts have been devoted to the development of D–A-conjugated polymers based on the dialkyl/dialkoxy-substituted BDT motifs, to the best of our

Received: August 31, 2012
Accepted: November 13, 2012
Published: November 13, 2012

knowledge, there are only a very few reports of D−π-A-conjugated small-molecule-containing dialkoxy-substituted BDT being used for solution-processed organic solar cells.[16,17]

In an attempt to expand the scope of the BDT unit for solution-processed small-molecule organic solar cells, herein, we present the synthesis and photovoltaic performance of a new dialkoxy-substituted BDT containing a π-conjugated D−A organic small molecule, **BDT(TBT)$_2$**, consisting of dialkoxy-substituted BDT as the central donor unit and benzothiadiazole (BT) flanked by triphenylamine as the terminal conjugated segment. BT is one of the most promising acceptor units and has been used very often to construct D−A-conjugated polymers for PSC applications. Some of those D−A copolymers have demonstrated encouraging photovoltaic performances with PCEs exceeding 5%.[18−21] In addition to LBG conjugated copolymers, there are also many reports of using the BT unit as a promising constituent in π-conjugated D−A organic small molecules.[22−25] Particularly, small molecules containing BT as the acceptor unit and triphenylamine as the donor segment in both linear and star-shaped molecular architectures have been widely explored as promising active materials in small-molecular organic solar cell research in recent literature.[26−30] Triphenylamine was combined with the BT unit to take advantage of its good electron-donating and hole-transporting properties, as well as its three-dimensional propeller structures.[31] By combining BT and triphenylamine units together with a thiophene(C10)-bridged naphtho[1,2-*b*:5,6-*b*′]dithiophene (NDT) donor unit, we have developed, more recently, one new small molecule that has delivered a promising photovoltaic performance with a PCE of 2.20%.[32] We further envisioned that replacing the thiophene(C10)-bridged NDT donor unit with the BDT unit may result in an even better photovoltaic performance because the BDT unit can form better π−π stacking owing to its larger planar structure with minimal steric hindrance with the adjacent units compared to a thiophene(C10)-bridged NDT donor unit, thus offering higher charge generation and transport and concomitantly favoring lower highest occupied molecular orbital (HOMO) levels for higher V_{oc}. Thus, the small molecule **BDT(TBT)$_2$** was conveniently synthesized in high yield using the Stille coupling reaction. A detailed investigation of its thermal, photophysical, and electrochemical properties was carried out. The potential of **BDT(TBT)$_2$** in organic field-effect transistor (OFET) and OPV devices has been evaluated and presented.

EXPERIMENTAL SECTION

Materials and Synthesis. 2,6-Bis(trimethyltin)-4,8-bis-(ethylhexyloxy)benzo[1,2-*b*:4,5-*b*′]dithiophene (**4**) was prepared following a procedure described in the literature.[33] 4,7-Dibromobenzo-[*c*-1,2,5]thiadiazole (**2**), 4-(diphenylamino)phenylboronic acid (**1**), anhydrous chlorobenzne (99.8%), and tri-*o*-tolylphosphine [P(*o*-tol)$_3$] were purchased from Aldrich. Tris(dibenzylideneacetone)-dipalladium(0) [$Pd_2(dba)_3$] and tetrakis(triphenylphosphine)-palladium(0) [$Pd(PPh_3)_4$] were obtained from Strem Chemicals. All other chemicals were reagent grade and were obtained from commercial sources (Fluka, Acros, and TCI) and used as-received without further purification unless stated otherwise.

*[4-(7-Bromobenzo[1,2,5]thiadiazol-4-yl)phenyl]diphenylamine (**3**).* In a 50 mL flame-dried two-necked flask, **2** (1 g, 3.4 mmol), **1** (1 g, 3.4 mmol), and $Pd(PPh_3)_4$ (0.2 g, 0.16 mmol) were added and subjected to three vacuum/nitrogen fill cycles. Nitrogen-degassed toluene (18 mL) and an aqueous 2 M K_2CO_3 solution (6 mL) were subsequently added. The reaction mixture was heated to reflux for 24 h and was monitored by thin-layer chromatography. After 24 h, water was added to quench the reaction and the organic layer was extracted with dichloromethane. Dichloromethane was subsequently removed under reduced pressure. The resulting crude product was purified by column chromatography, eluting with hexane/CH_2Cl_2 (4:1) to produce compound **3** as a yellow solid (0.90 g, 58%). ^{1}H NMR (400 MHz, $CDCl_3$): δ 7.89−7.87 (d, 1H), 7.86−7.73 (d, 1H), 7.80−7.78 (d, 2H), 7.53−7.28 (d, 2H), 7.28−7.05 (m, 10H). ^{13}C NMR ($CDCl_3$, 100 MHz): δ 153.95, 147.48, 132.34, 129.88, 129.82, 129.38, 129.33, 127.39, 127.28, 125.02, 124.87, 123.49, 122.92, 112.17. Elem anal. Calcd for $C_{24}H_{16}BrN_3S$, C, 62.89; H, 3.52; S, 7.00. Found: C, 62.94; H, 3.59; S, 6.88.

BDT(TBT)$_2$. The title small molecule **BDT(TBT)$_2$** was prepared as follows: A mixture of compound **3** (0.317 g, 0.70 mmol), compound **4** (0.2 g, 0.272 mmol), $Pd_2(dba)_3$ (12.6 mg, 5 mol %), and P(*o*-tolyl)$_3$ (8.4 mg, 10 mol %) was added to a 50 mL flame-dried two-necked flask and subjected to three vacuum/argon fill cycles. Argon-degassed chlorobenzene (9 mL) was added, and the mixture was stirred for 20 min with flushing argon. The reaction mixture was heated to reflux for 24 h. After completion of the reaction, chlorobenzene was removed under reduced pressure, and the residue was purified by passing it through a column of silica gel using hexane/CH_2Cl_2 (6:1) as the eluent to yield compound **BDT(TBT)$_2$** (0.236 g, 71%) as a dark-brown solid. ^{1}H NMR (400 MHz, $CDCl_3$): δ 8.74 (s, 2H), 7.91−7.89 (d, 2H), 7.82−7.80 (d, 4H), 7.67−7.65 (d, 2H), 7.25−6.98 (m, 24H), 4.27−4.26 (d, 4H), 1.87−1.39 (m, 14H), 1.18−0.90 (m, 14H). ^{13}C NMR (100 MHz, $CDCl_3$): δ 159.92, 152.89, 148.10, 147.35, 144.68, 138.81, 133.30, 13041, 129.87, 129.33, 129.20, 127.35, 126.90, 125.43, 124.97, 124.85, 123.37, 123.26, 122.91, 122.57, 121.96, 40.79, 30.65, 29.37, 23.99, 23.28, 14.31, 11.55. Elem anal. Calcd for $C_{74}H_{68}N_6O_2S_4$: C, 73.97; H, 5.70; N, 6.99; O, 2.66; S, 10.67. Found: C, 73.89; H, 5.67; N, 7.05; O, 2.72; S, 10.68.

General Instrumentation. ^{1}H and ^{13}C NMR spectra were recorded on a JEOL FT-NMR (400 MHz) spectrophotometer using $CDCl_3$ as the solvent. Chemical shifts were reported as δ values (ppm) relative to the internal standard tetramethylsilane. Elemental analyses were carried out using a CE Instruments Flash EA 1112 series analyzer. The UV−vis absorption spectral films or solutions were obtained using a Shimadzu UV-2550 spectrophotometer. Photoluminescence (PL) spectra of the films were obtained using a Jasco FP-6500 spectrophotometer. Thermogravimetric analysis (TGA) was carried out with a TA Instruments Q-50 analyzer at a scanning rate of 10 °C min^{-1} under a nitrogen atmosphere. The temperature of degradation (T_d) corresponded to a 5% weight loss. Differential scanning calorimetry (DSC) experiments were performed on a TA Instruments DSC 2910 calorimeter at a heating rate of 10 °C min^{-1} under a nitrogen atmosphere. Cyclic voltammetry (CV) measurements were performed on a VersaSTAT3 (METEK) under argon at a scan rate of 50 mV s^{-1} at room temperature, wherein a platinum wire and Ag/AgCl were used as the counter and reference electrodes, respectively. The reference electrode was calibrated with Fc/Fc$^+$ as an external standard. The samples were prepared in a chloroform solution with 0.10 M tetrabutylammonium hexafluorophosphate (*n*-Bu_4NPF_6) as the electrolyte. Thin-film X-ray diffraction (XRD) patterns were recorded using a PANalytical X-Pert diffractometer operating at 30 kV and 20 mA with Cu Kα radiation (λ = 1.5405 Å) at a scan speed of 1° min^{-1} and a step size of 0.04°. The measurements were obtained in a scanning interval of 2θ between 1° and 30°. The film samples were fabricated by drop-casting on a silicon wafer, followed by drying under vacuum (solvent, chloroform; solution concentration, 10 mg mL^{-1}). The surface morphology was measured using a Digital Instruments multimode atomic force microscope controlled by a Nanoscope IIIa scanning probe microscope 20 controller.

Organic Thin-Film Transistor (OTFT) Device Fabrication and Characterization. OTFT devices were fabricated in a bottom-contact geometry (channel length = 12 μm; width = 120 μm). The source and drain contacts consisted of gold (100 nm), and the dielectric was silicon oxide (SiO_2) with a thickness of 300 nm. The SiO_2 surface was cleaned, dried, and pretreated with a solution of 10 mM octyltrichlorosilane (OTS-8) in toluene at room temperature for 2 h

Scheme 1. Synthetic Route to the Intermediate and BDT(TBT)$_2$

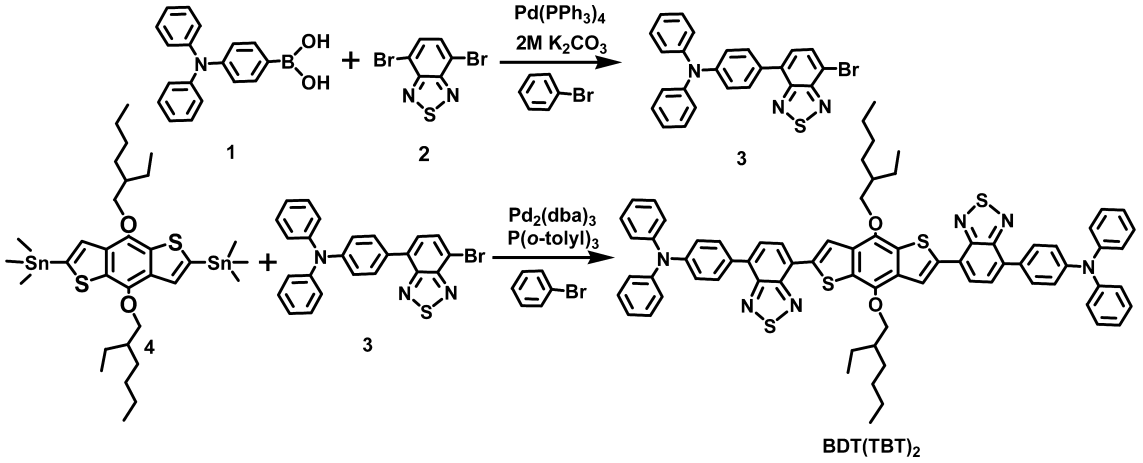

under nitrogen to produce nonpolar and smooth surfaces onto which the small molecule could be spin-coated. The small molecule **BDT(TBT)$_2$** was dissolved to a concentration of 0.5 wt % in chloroform. Films of the organic semiconductor were spin-coated at 1500 rpm for 50 s to a thickness of 50 nm, followed by an annealing process. The electrical characteristics of the OFETs were measured under ambient conditions using a Keithley 4200 unit. The field-effect mobilities were calculated in the saturation regime using the equation $ID = (W/2L)\mu C_i(V_G - V_T)^2$, where I_D is the drain current in the saturated regime, W and L are the channel width and length, respectively, μ is the field-effect mobility, C_i is the capacitance per unit area of the gate dielectric layer, and V_G and V_T are the gate and threshold voltages, respectively.

Photovoltaic Device Fabrication and Characterization. All of the OPV cells were prepared on a commercial indium–tin oxide (ITO)-coated glass substrate with a sandwiched structure of glass/ITO/PEDOT:PSS/**BDT(TBT)$_2$**:$PC_{71}BM$/LiF/Al. Prior to use, the patterned ITO-covered glass substrates were cleaned with deionized water, acetone, and isopropyl alcohol using ultrasonication, followed by treatment with UV and O_3. PEDOT:PSS (AI 4083, H. C. Starck) was spin-coated (2600 rpm, 40 s) onto the cleaned ITO glass at a thickness of 40 nm, dried at 140 °C for 20 min in the atmosphere, and then transferred into the glovebox filled with dinitrogen. Blends of **BDT(TBT)$_2$** and $PC_{71}BM$ (Nano-C, USA) with different weight ratios (from 1:0.5 to 1:4 w/w) were solubilized overnight in a chlorobenzene (concentration: 20 mg mL^{-1}) or chloroform (concentration: 10 mg mL^{-1}) solution, filtered through a 0.45-μm poly(tetrafluoroethylene) filter, and subsequently spin-coated at 700 (for chlorobenzene)/1400 (for chloroform) rpm for 60 s (thickness, 60–70 nm) onto the PEDOT:PSS layer of the ITO. The resulting films were dried at room temperature for 20 min under nitrogen and then under vacuum for 12 h. The devices were completed by the deposition of a 0.5-nm layer of LiF and a 120-nm layer of aluminum. These layers were thermally evaporated at a pressure of 1×10^{-6} Torr at room temperature. The active area of every device was 9 mm^2. The current–voltage (J–V) characteristics of the photovoltaic devices were measured in the dark and under white-light illumination at AM 1.5G using a solar simulator (Newport) at 100 mW cm^{-2}, adjusted with a standard PV reference (2 × 2 cm) and a monocrystalline silicon solar cell (calibrated at NREL, USA) with a Keithley 2400 source-measure unit. The external quantum efficiency (EQE) was determined using a Polaronix K3100 spectrometer.

RESULTS AND DISCUSSION

Synthesis and Thermal Stability. The synthesis of **BDT(TBT)$_2$** involves straightforward synthetic reactions, as depicted in Scheme 1. Intermediate **3** with triarylamine at one end was synthesized by a selective Suzuki coupling between **1** and **2**. **4** was prepared following a procedure described in the literature.[33] **BDT(TBT)$_2$** was synthesized via a $Pd_2(dba)_3$-catalyzed Stille coupling between **3** and **4**. Detailed synthetic procedures and compound characterizations are described further in the Experimental Section. TGA of **BDT(TBT)$_2$** revealed a high T_d (5% weight loss) of 298 °C, indicating a thermal stability appropriate for long-term photovoltaic application (Figure 1). As if evident from DSC analysis (Figure 1, inset), **BDT(TBT)$_2$** has a tendency to crystallize because it possesses a prominent melting temperature (T_m) at 254.1 °C (in the heating cycle) and an isotropic-to-crystalline transition (T_c) at 153.1 °C (in the cooling cycle), although lacking a distinct glass transition temperature (T_g).

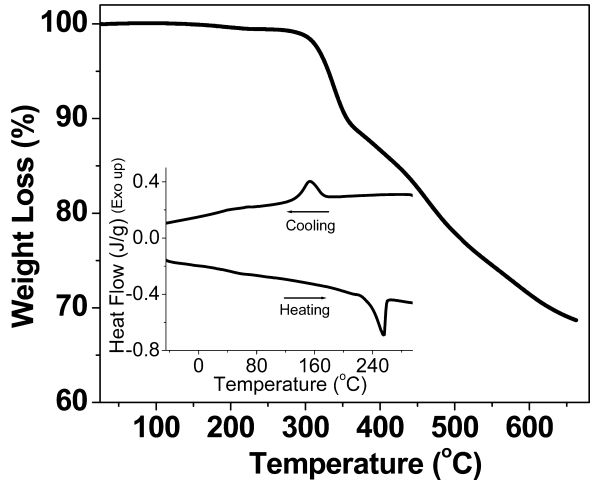

Figure 1. TGA curves of **BDT(TBT)$_2$** with a heating rate of 10 °C min^{-1} under a nitrogen atmosphere. Inset: DSC traces of **BDT(TBT)$_2$** at a scanning rate of 10 °C min^{-1} in the second heating and cooling cycles.

Optical Properties (Table 1). UV–vis absorption spectra for **BDT(TBT)$_2$** in a chlorobenzene solution and as a thin film are shown in Figure 2a. The **BDT(TBT)$_2$** solution displayed an absorption band in the range of around 300–600 nm, with the longest wavelength absorption maximum at 527 nm. Compared with the solution absorption spectrum, the visible absorption band of the **BDT(TBT)$_2$** film was broadened and red-shifted (~22 nm). The red shift and broader absorption could be attributed to the well-ordered π–π stacking of **BDT(TBT)$_2$** in the solid state.[34] The film absorption onset was observed at 650

Table 1. Optical and Electrochemical Properties of BDT(TBT)$_2$

	solution	film				
small molecule	λ_{max} (nm)[a]	λ_{max} (nm)[b]	λ_{onset} (nm)[b]	E_g^{opt} (eV)[c]	E_{ox}[d] (V)/E_{HOMO}[e] (eV)	E_{red}[d] (V)/E_{LUMO}[e] (eV)
BDT(TBT)$_2$	527	549	652	1.90	1.04/−5.44 ± 0.01	−1.03/−3.37 ± 0.01

[a]Measured in a chlorobenzene solution. [b]Spin-coated film from a chlorobenzene solution. [c]Optical band gap, $E_g^{opt} = 1240/(\lambda_{onset})_{film}$. [d]Potential determined by CV in 0.10 M Bu_4NPF_6/CH_3CN. [e]$E_{HOMO} = -e(4.4 + E_{onset}^{ox})$ (eV). [f]$E_{LUMO} = -e(4.4 + E_{onset}^{red})$ (eV).

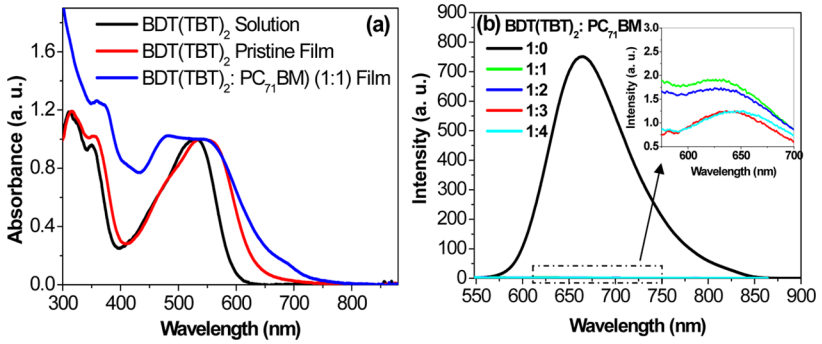

Figure 2. (a) UV−vis absorption spectra of **BDT(TBT)$_2$** in chlorobenzene and in the solid state. (b) PL spectra of **BDT(TBT)$_2$** and a **BDT(TBT)$_2$**/$PC_{71}BM$-blended thin film.

nm, corresponding to an optical band gap (E_g^{opt}) of 1.90 eV. As is further shown in Figure 2a, $PC_{71}BM$ can compensate for the absorption valley in the range of ~300−520 nm. The PL spectrum of **BDT(TBT)$_2$** shown in Figure 2b had a distinct strong emission band with an emission maximum at 664 nm. In blends with $PC_{71}BM$ for films with different weight ratios (1:1 to 1:4), luminescence from **BDT(TBT)$_2$** was found to be almost completely quenched because of a favorable ultrarapid charge transfer from the small molecule to PCBM.

Electrochemical Properties (Table 1). CV was used to investigate the electrochemical properties of the small molecule. Figure 3 presents a cyclic voltammogram of the **BDT(TBT)$_2$** film. The onset potential for the oxidation of **BDT(TBT)$_2$** was located around 1.04 V versus the Ag/AgCl reference electrode, which corresponded to a HOMO energy level of −5.44 ± 0.01 eV. The lowest unoccupied molecular orbital (LUMO) was estimated to be −3.37 ± 0.01 eV, based on the onset potential for reduction at −1.03 V. A comparative energy diagram of **BDT(TBT)$_2$** and $PC_{71}BM$ is further presented in the inset of Figure 3. It is worth noting that the HOMO level of **BDT(TBT)$_2$** not only is deep-lying for greater oxidative stability but also is in good agreement with the theoretically predicted ideal HOMO level to obtain a higher open-circuit voltage (V_{oc}) for better performance in a photovoltaic cell.[35a] The LUMO also is seen being positioned well above the LUMO level of $PC_{71}BM$ (−3.91 eV)[35b] with the desired energy offset ΔE_{LUMO} ($E_{LUMO(A)} - E_{LUMO(D)}$) > 0.3 eV, ensuring efficient exciton dissociation and charge separation.[35a]

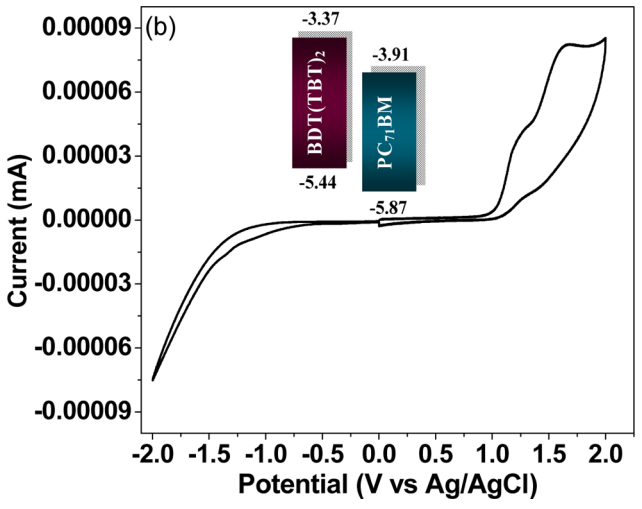

Figure 3. Cyclic voltammogram of the **BDT(TBT)$_2$** film in a 0.1 mol L^{-1} Bu_4NPF_6/CH_3CN solution at a scan rate of 50 mV s^{-1}. Inset: Energy level diagram showing the HOMO and LUMO energy levels of **BDT(TBT)$_2$** and $PC_{71}BM$.

XRD. The XRD patterns of **BDT(TBT)$_2$** films were recorded both before and after annealing to elucidate molecular ordering in the solid state, with the results presented in Figure 4. While the as-cast film showed a weak, sharp peak at 2θ of 7.78°, the film after undergoing annealing at 160 °C resulted a strong, intense peak centered at 2θ of 8.10° corresponding to an interlayer d spacing (d_1) of 10.90 Å that is smaller than twice the length of the ethylhexyl chain of ca. 12.76 Å in its most extended conformation,[36] which implies that the small

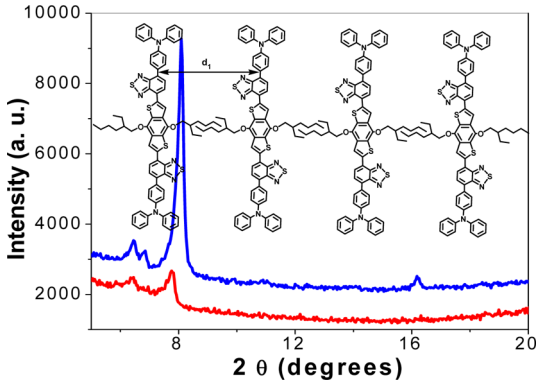

Figure 4. XRD patterns of the **BDT(TBT)$_2$** as-cast film and film after annealing at 160 °C. Inset: Schematic representation of the molecular packing of **BDT(TBT)$_2$** in the solid state.

dx.doi.org/10.1021/am301841p | ACS Appl. Mater. Interfaces 2012, 4, 6669−6675

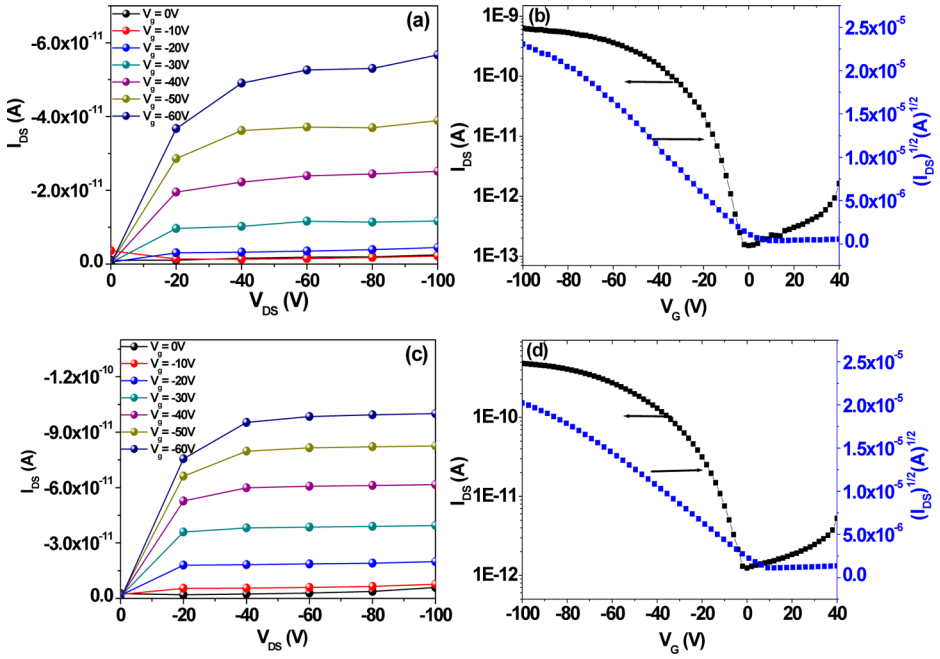

Figure 5. Current–voltage characteristics (I_{DS} vs V_{DS}) at different gate voltages (V_G) and transfer curves for BDT(TBT)$_2$-based TFT devices at room temperature (a and b) and after annealing at 180 °C (c and d).

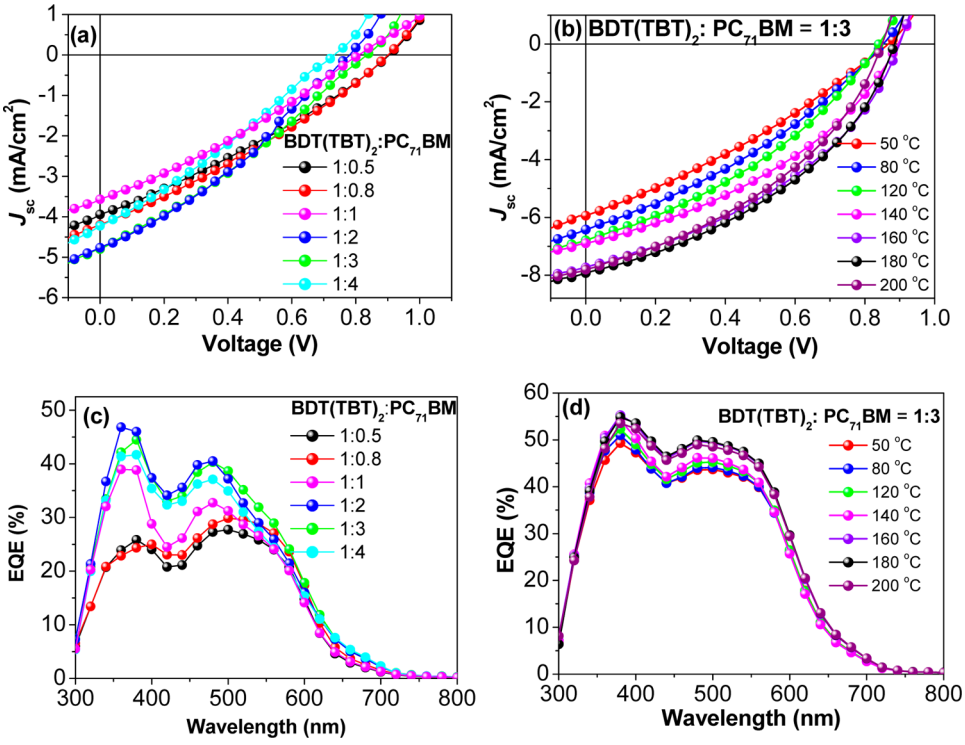

Figure 6. *J*–*V* curves of Barrett–Halenda–Joyner solar cell devices based on **BDT(TBT)$_2$**/PC$_{71}$BM composites from a chlorobenzene solution (a) at different weight ratios (1:0.5 to 1:4) before annealing and (b) at the 1:3 ratio after annealing (at different temperatures) under AM 1.5G, 100 mW cm^{-2}. (c and d) EQE profiles of the corresponding devices.

molecule has an interdigitated assembly of alkyl chains (as shown in the inset of Figure 4). Unlike the cast **BDT(TBT)$_2$** film, the thermally annealed film exhibited an additional weak peak toward wider angles with a half-width peak maximum of ~16.19° (*d* spacing; d_2 of 5.47 Å), assignable to the cofacial interlayer π–π stacking between the conjugated main chains. The shift in the diffraction angle and increase in the peak intensity with concomitant emergence of a new peak toward the higher-angle region indicates that thermal annealing of **BDT(TBT)$_2$** produces a well-organized assembly and improved crystallinity in the molecular film with closer interdigitation of the branched ethylhexyl side chains.

Field-Effect Transistor Characteristics. The field-effect mobility of **BDT(TBT)$_2$** was evaluated by fabricating thin-film

dx.doi.org/10.1021/am301841p | *ACS Appl. Mater. Interfaces* 2012, 4, 6669–6675

transistors (TFTs) with bottom-gate, top-contact device configurations. The detailed device fabrication process is described in the Experimental Section. Figure 5 exhibits the characteristic transfer and output plots of transistors fabricated from **BDT(TBT)$_2$** films both at room temperature and with annealing at 180 °C. The hole mobility of **BDT(TBT)$_2$** at room temperature was found to be 1.4×10^{-6} cm^2 V^{-1} s^{-1} with an I_{on}/I_{off} ratio of 10^3, while annealing at 180 °C for 10 min improved the mobility to 2.7×10^{-6} cm^2 V^{-1} s^{-1} with an I_{on}/I_{off} ratio of 10^3 due to better packing of the **BDT(TBT)$_2$** film at higher temperature, corroborating the results of the XRD studies.

Photovoltaic Properties. To explore the potential use of **BDT(TBT)$_2$** in organic solar cells, the photovoltaic cells were fabricated from a chlorobenzene solution at an active layer thickness of 50−55 nm using **BDT(TBT)$_2$** as the donor and $PC_{71}BM$ as the acceptor with the device architecture ITO/PEDOT:PSS/**BDT(TBT)$_2$**:$PC_{71}BM$/LiF/Al. During a preliminary study based on **BDT(TBT)$_2$** as a new donor small molecule, we maintained the composite weight ratios of **BDT(TBT)$_2$**/$PC_{71}BM$ in the active layers between 1:0.5 and 1:4 (w/w). The $J-V$ curves for the corresponding cells are presented in Figure 6a, and the device parameters of the respective cells have been compiled in Table 2. Even though

Table 2. Summary of the Photovoltaic Performance of Solution-Processed Organic Solar Cells based on BDT(TBT)$_2$/$PC_{71}BM$ blends (Active Layer Thickness ~ 55 nm) in Chlorobenzene with and without Annealing

active layer	J_{sc} (mA cm^{-2})	V_{oc} (V)	FF	PCE (%)
BDT(TBT)$_2$/$PC_{71}BM$ (1:0.5, as cast)	3.94	0.90	0.30	1.06
BDT(TBT)$_2$/$PC_{71}BM$ (1:0.8, as cast)	4.20	0.90	0.30	1.12
BDT(TBT)$_2$/$PC_{71}BM$ (1:1, as cast)	3.56	0.81	0.30	0.85
BDT(TBT)$_2$/$PC_{71}BM$ (1:2, as cast)	4.77	0.78	0.32	1.18
BDT(TBT)$_2$/$PC_{71}BM$ (1:3, as cast)	4.80	0.83	0.29	1.18
BDT(TBT)$_2$/$PC_{71}BM$ (1:4, as cast)	4.22	0.73	0.29	0.88
BDT(TBT)$_2$/$PC_{71}BM$ (1:3, 50 °C annealing)	5.94	0.87	0.31	1.58
BDT(TBT)$_2$/$PC_{71}BM$ (1:3, 80 °C annealing)	6.42	0.85	0.33	1.80
BDT(TBT)$_2$/$PC_{71}BM$ (1:3, 120 °C annealing)	6.80	0.84	0.36	2.03
BDT(TBT)$_2$/$PC_{71}BM$ (1:3, 140 °C annealing)	6.90	0.90	0.38	2.35
BDT(TBT)$_2$/$PC_{71}BM$ (1:3, 160 °C annealing)	7.73	0.90	0.39	2.74
BDT(TBT)$_2$/$PC_{71}BM$ (1:3, 180 °C annealing)	7.94	0.89	0.40	2.83
BDT(TBT)$_2$/$PC_{71}BM$ (1:3, 200 °C annealing)	7.81	0.85	0.39	2.60

the devices with active layer ratios of 1:2 and 1:3 provided the most promising results with identical PCE values of 1.18%, the active layer with the 1:3 ratio contributed both a higher V_{oc} and a higher J_{sc} compared to an analogous device with the 1:2 ratio. Because it was recognized from the XRD studies that annealing of the **BDT(TBT)$_2$** film resulted in a more organized assembly and greater crystallinity, which eventually could be favorable for improvements in J_{sc} and FF, a further attempt to enhance the device performance with the 1:3 **BDT(TBT)$_2$**/$PC_{61}BM$ ratio through optimization of the annealing temperature was performed. Figure 6b displays the $J-V$ curves of cells prepared from the active layers with the 1:3 ratio after annealing at different temperatures for 10 min. The corresponding solar cell device parameters are further listed in Table 2. Indeed, thermal annealing led to significant improvement in all three device parameters, i.e., J_{sc}, V_{oc}, and FF, and, in turn, facilitated the **BDT(TBT)$_2$** delivery of a significant photovoltaic performance with a maximum PCE up to 2.83% at 180 °C. It is worth noting that, with a desirable deep-lying ideal HOMO value of −5.44 ± 0.01 eV, two of the solar cell devices (Table 2) based on **BDT(TBT)$_2$** and $PC_{71}BM$ exhibited a noticeably high V_{oc} up to 0.9 V. The EQE curves of the corresponding cells, as shown in Figure 6c,d, indicate an efficient PCE from 300 to 700 nm with a maximum EQE value as high as 55% for the cell annealed at 180 °C.

CONCLUSIONS

In conclusion, a new, simple, yet efficient, alkyoxy-substituted BDT containing a D−π-A-conjugated small molecule, **BDT(TBT)$_2$**, was designed and synthesized. **BDT(TBT)$_2$** offers excellent solubility, thermal stability, a medium optical band gap of 1.90 eV, and an ideal deep-lying HOMO level of −5.44 ± 0.01 eV. Moreover, with a favorable highly ordered π-stacked structure upon thermal annealing, solution-processed organic solar cells composed of **BDT(TBT)$_2$** and $PC_{71}BM$ resulted in a modest PCE of ~2.83% with a high V_{oc} of 0.89 V during preliminary trials and also delivered a rarely observed 140% improvement in PCE compared to the untreated film. The results of our preliminary studies suggest that the small-molecule **BDT(TBT)$_2$** holds promise for efficient solution-processed small-molecular photovoltaic cells. We further envision that a higher PCE could be accomplished from alkyoxy-substituted BDT-based small molecules provided a more suitable molecular design that balances the compromise between LBG and favorable HOMO−LUMO energy relationship of the small-molecule donor and PCBM acceptor can be achieved.

AUTHOR INFORMATION

Corresponding Author

*Telephone: +063-270-2435. Fax: +063-270-2306. E-mail: shlee66@jbnu.ac.kr.

Notes

The authors declare no competing financial interest.

ACKNOWLEDGMENTS

This work was supported by the New & Renewable Energy program of the Korea Institute of Energy Technology Evaluation and Planning grant (No. 20103020010050) funded by the Ministry of Knowledge Economy, Republic of Korea.

REFERENCES

(1) Li, G.; Zhu, R.; Yang, Y. *Nat. Photonics* **2012**, *6*, 153.

(2) (a) He, Z.; Zhong, C.; Huang, X.; Wong, W.; Wu, H.; Chen, L.; Su, S.; Cao, Y. *Adv. Mater.* **2011**, *23*, 4636. (b) Dou, L. T.; You, J. B.; Yang, J.; Chen, C.-C.; He, Y. J.; Murase, S.; Moriarty, T.; Emery, K.; Li, G.; Yang, Y. *Nat. Photonics* **2012**, *6*, 180.

(3) (a) Small, C. E.; Chen, S.; Subbiah, J.; Amb, C. M.; Tsang, S.-W.; Lai, T.-H.; Reynolds, J. R.; So, F. *Nat. Photonics* **2012**, *6*, 115. (b) Li, X. H.; Choy, W. C. H.; Huo, L. J.; Xie, F. X.; Sha, W. E. I.; Ding, B. F.; Guo, X.; Li, Y. F.; Hou, J. H.; You, J. B.; Yang, Y. *Adv. Mater.* **2012**, *24*, 3046. (c) Chen, S.; Small, C. E.; Amb, C. M.; Subbiah, J.; Lai, T. H.; Tsang, S. W.; Manders, J. R.; Reynolds, J. R.; So, F. *Adv. Energy Mater.* **2012**, DOI: 10.1002/aenm.201200184.

(4) (a) Loser, S.; Bruns, C. J.; Miyauchi, H.; Ortiz, R. P.; Facchetti, A.; Stupp, S. I.; Marks, T. J. *J. Am. Chem. Soc.* **2011**, *133*, 8142. (b) Loser, S.; Miyauchi, H.; Hennek, J. W.; Smith, J.; Huang, C.; Facchetti, A.; Marks, T. J. *Chem. Commun.* **2012**, *48*, 8511.
(5) (a) Zhou, J.; Wan, X.; Liu, Y.; Long, G.; Wang, F.; Li, Z.; Zuo, Y.; Li, C.; Chen, Y. *Chem. Mater.* **2011**, *23*, 4666. (b) Li, Z.; He, G.; Wan, X.; Liu, Y.; Zhou, J.; Long, G.; Zuo, Y.; Zhang, M.; Chen, Y. *Adv. Energy Mater.* **2012**, *2*, 74.
(6) (a) Burckstummer, H.; Kronenberg, N. M.; Gsanger, M.; Stolte, M.; Meerholz, K.; Wurthner, F. *J. Mater. Chem.* **2010**, *20*, 240. (b) Mayerhoffer, U.; Deing, K.; Gruss, K.; Braunschweig, H.; Meerholz, K.; Wurthner, F. *Angew. Chem., Int. Ed.* **2009**, *48*, 8776.
(7) (a) Rousseau, T.; Cravino, A.; Bura, T.; Ulrich, G.; Ziessel, R.; Roncali, J. *Chem. Commun.* **2009**, 1673. (b) Rousseau, T.; Cravino, A.; Ripaud, E.; Leriche, P.; Rihn, S.; De Nicola, A.; Ziessel, R.; Roncali, J. *Chem. Commun.* **2010**, *46*, 5082.
(8) (a) Tamayo, A. B.; Walker, B.; Nguyen, T.-Q. *J. Phys. Chem. C* **2008**, *112*, 11545. (b) Tamayo, A. B.; Dang, X.-D.; Walker, B.; Seo, J. H.; Kent, T.; Nguyen, T.-Q. *Appl. Phys. Lett.* **2009**, *24*, 103301. (c) Walker, B.; Tamayo, A. B.; Dang, X. D.; Zalar, P.; Seo, J. H.; Garcia, A.; Tantiwiwat, M.; Nguyen, T.-Q. *Adv. Funct. Mater.* **2009**, *19*, 3063. (d) Zhang, Y.; Dang, X.-D.; Kim, C.; Nguyen, T.-Q. *Adv. Energy Mater.* **2011**, *1*, 610.
(9) (a) Zhang, J.; Deng, D.; He, C.; He, Y.; Zhang, M.; Zhang, Z.-G.; Zhang, Z.; Li, Y. *Chem. Mater.* **2011**, *23*, 817. (b) Lin, Y.; Cheng, P.; Li, Y.; Zhan, X. *Chem. Commun.* **2012**, *48*, 4773. (c) Lin, Y.; Li, Y.; Zhan, X. *Chem. Soc. Rev.* **2012**, *41*, 4245.
(10) (a) Sun, Y.; Welch, G. C.; Leong, W. L.; Takacs, C. J.; Bazan, G. C.; Heeger, A. J. *Nat. Mater.* **2011**, *11*, 44. (b) Poll, T. S.; Love, J. A.; Nguyen, T. Q.; Bazan, G. C. *Adv. Mater.* **2012**, *24*, 3646.
(11) (a) Liang, Y. Y.; Yu, L. P. *Acc. Chem. Res.* **2010**, *43*, 1227. (b) Liang, Y. Y.; Xu, Z.; Xia, S.-T.; Tsai, Y.; Wu, G.; Li, G.; Ray, C.; Yu, L. *Adv. Mater.* **2010**, *22*, E135. (c) Son, H. J.; Wang, W.; Xu, T.; Liang, Y.; Wu, Y.; Li, G.; Yu, L. *J. Am. Chem. Soc.* **2011**, *133*, 1885.
(12) Zhou, H.; Yang, L.; Stuart, A. C.; Price, S. C.; Liu, S.; You, W. *Angew. Chem., Int. Ed.* **2011**, *50*, 2995.
(13) Price, S. C.; Stuart, A. C.; Yang, L.; Zhou, H.; You, W. *J. Am. Chem. Soc.* **2011**, *133*, 4625.
(14) (a) Huo, L.; Zhang, S.; Guo, X.; Xu, F.; Li, Y.; Hou, J. *Angew. Chem., Int. Ed.* **2011**, *50*, 9697. (b) Huang, Y.; Guo, X.; Liu, F.; Huo, L.; Chen, Y.; Russell, T. P.; Han, C. C.; Li, Y.; Hou, J. *Adv. Mater.* **2012**, *24*, 3383.
(15) He, Z.; Zhong, C.; Huang, X.; Wong, W.-Y.; Wu, H.; Chen, L.; Su, S.; Cao, Y. *Adv. Mater.* **2011**, *23*, 4636.
(16) (a) Liu, Y.; Wan, X.; Wang, F.; Zhou, J.; Long, G.; Tian, J.; Chen, Y. *Adv. Mater.* **2011**, *23*, 4666. (b) Zhou, J.; Wan, X.; Liu, Y.; Zuo, Y.; Li, Z.; He, G.; Long, G.; Ni, W.; Li, C.; Su, X.; Chen, Y. *J. Am. Chem. Soc.* **2012**, *134*, 16345.
(17) Lee, O. P.; Yiu, A. T.; Beaujuge, P. M.; Woo, C. H.; Holcombe, T. W.; Millstone, J. E.; Douglas, J. D.; Chen, M. S.; Fréchet, J. M. J. *Adv. Mater.* **2011**, *23*, 5359.
(18) Park, S. H.; Roy, A.; Beaupré, S.; Cho, S.; Coates, N.; Moon, J. S.; Moses, D.; Leclerc, M.; Lee, K.; Heeger, A. J. *Nat. Photonics* **2009**, *3*, 297.
(19) Peet, J.; Kim, J. Y.; Coates, N. E.; Ma, W. L.; Moses, D.; Heeger, A. J.; Bazan, G. C. *Nat. Mater.* **2007**, *6*, 497.
(20) Wang, E. G.; Wang, L.; Lan, L. F.; Luo, C.; Zhuang, W. L.; Peng, J. B.; Cao, Y. *Appl. Phys. Lett.* **2008**, *92*, 033307.
(21) Hou, J. H.; Chen, H. Y.; Zhang, S. Q.; Li, G.; Yang, Y. *J. Am. Chem. Soc.* **2008**, *130*, 16144.
(22) Chen, J. J.-A.; Chen, T. L.; Kim, B.; Poulsen, D. A.; Mynar, J. L.; Fréchet, J. M. J.; Ma, B. *ACS Appl. Mater. Interfaces* **2010**, *2*, 2679.
(23) Zhao, X.; Piliego, C.; Kim, B.; Poulsen, D. A.; Ma, B.; Unruh, D. A.; Fréchet, J. M. J. *Chem. Mater.* **2010**, *22*, 2325.
(24) Steinberger, S.; Mishra, A.; Reinold, E.; Levichkov, J.; Uhrich, C.; Pfeiffer, M.; Baüerle, P. *Chem. Commun.* **2011**, *47*, 1982.
(25) Lin, L. Y.; Lu, C. W.; Huang, W. C.; Chen, Y. H.; Lin, H. W.; Wong, K. T. *Org. Lett.* **2011**, *13*, 4962.
(26) Shang, H.; Fan, H.; Liu, Y.; Hu, W.; Li, Y.; Zhan, X. *Adv. Mater.* **2011**, *23*, 1554.
(27) Li, W.; Du, C.; Li, F.; Zhou, Y.; Fahlman, M.; Bo, Z.; Zhang, F. *Chem. Mater.* **2009**, *21*, 5327.
(28) Zhang, J.; Yang, Y.; He, C.; He, Y.; Zhao, G.; Li, Y. *Macromolecules* **2009**, *42*, 7619.
(29) He, C.; He, Q.; Yi, Y.; Wu, G.; Bai, F.; Shuaia, Z.; Li, Y. *J. Mater. Chem.* **2008**, *18*, 4085.
(30) Yang, Y.; Zhang, J.; Zhou, Y.; Zhao, G.; He, C.; Li, Y.; Andersson, M.; Inganäs, O.; Zhang, F. *J. Phys. Chem. C* **2010**, *114*, 3701.
(31) Ning, Z.; Tian, H. *Chem. Commun.* **2009**, 5483.
(32) Dutta, P.; Yang, W.; Eom, S. H.; Lee, W. H.; Kang, I. N.; Lee, S.-H. *Chem. Commun.* **2012**, *48*, 573.
(33) Liang, Y.; Feng, D.; Wu, Y.; Tsai, S. T.; Li, G.; Ray, C.; Yu, L. *J. Am. Chem. Soc.* **2009**, *131*, 7792.
(34) Huo, L.; Guo, X.; Li, Y.; Hou, J. *Chem. Commun.* **2011**, *47*, 8850.
(35) (a) Scharbar, M. C.; Mühlbacher, D.; Koppe, M.; Denk, P.; Waldauf, C.; Hegger, A. J.; Barbec, C. J. *Adv. Mater.* **2006**, *18*, 789. (b) He, Y.; Li, Y. F. *Phys. Chem. Chem. Phys.* **2011**, *13*, 1970.
(36) The length of the ethylhexyl chain was calculated using the *MM2* program of *ChemDraw* (Chem3D Ultra 9.0).